OFFICE OF NAVAL RESEARCH

Statistical Fine Structure in the
Inhomogeneously Broadened Electronic Origin
of Pentacene in p-Terphenyl

by

T. P. Carter, M. Manavi, and W. E. Moerner

Prepared for Publication

in

Journal of Chemical Physics

IBM Research Division
Almaden Research Center
650 Harry Road
San Jose, California 95120-6099

DTIC
ELECTE
FEB 1 1 1988
H

January 29, 1988

88 2 05 008

Unclassified

A191211

SECURITY CLASSIFICATION OF THIS PAGE

REPORT DOCUMENTATION PAGE

1a. REPORT SECURITY CLASSIFICATION	1b. RESTRICTIVE MARKINGS
UNCLASSIFIED	

2a. SECURITY CLASSIFICATION AUTHORITY	3. DISTRIBUTION / AVAILABILITY OF REPORT
	This document has been approved for
2b. DECLASSIFICATION / DOWNGRADING SCHEDULE	public release and sale; its distribution is unlimited.

4. PERFORMING ORGANIZATION REPORT NUMBER(S)	5. MONITORING ORGANIZATION REPORT NUMBER(S)
Technical Report #15	

6a. NAME OF PERFORMING ORGANIZATION	6b. OFFICE SYMBOL (If applicable)	7a. NAME OF MONITORING ORGANIZATION
IBM Research Division Almaden Research Center		Office of Naval Research

6c. ADDRESS (City, State, and ZIP Code)	7b. ADDRESS (City, State, and ZIP Code)
650 Harry Road San Jose, CA 95120-6099	Chemistry Division Code 1113 Arlington, VA 22217

8a. NAME OF FUNDING / SPONSORING ORGANIZATION	8b. OFFICE SYMBOL (If applicable)	9. PROCUREMENT INSTRUMENT IDENTIFICATION NUMBER
Office of Naval Research		N00014-84-C-0708

8c. ADDRESS (City, State, and ZIP Code)	10 SOURCE OF FUNDING NUMBERS			
Chemistry Division, Code 1113 Arlington, VA 22217	PROGRAM ELEMENT NO.	PROJECT NO.	TASK NO.	WORK UNIT ACCESSION NO

11. TITLE (Include Security Classification)
Statistical Fine Structure in the Inhomogeneously Broadened Electronic Origin of Pentacene in p-Terphenyl

12. PERSONAL AUTHOR(S)
T. P. Carter, M. Manavi, and W. E. Moerner

13a. TYPE OF REPORT	13b. TIME COVERED	14. DATE OF REPORT (Year, Month, Day)	15. PAGE COUNT
interim technical	FROM _____ TO _____	January 29, 1988	47

16. SUPPLEMENTARY NOTATION
submitted for publication in Journal of Chemical Physics

17.	COSATI CODES		18. SUBJECT TERMS (Continue on reverse if necessary and identify by block number)
FIELD	GROUP	SUB-GROUP	statistical fine structure, inhomogeneous broadening, molecular spectroscopy, defects in solids

19. ABSTRACT (Continue on reverse if necessary and identify by block number)
Recently, the first observation of statistical fine structure on an inhomogeneously broadened absorption profile was reported (W. E. Moerner, T. P. Carter, Phys. Rev. Lett. $\underline{59}$, 2705 (1987)) for mixed crystals of pentacene in p-terphenyl using laser FM spectroscopy. Statistical fine structure is time-independent structure on the inhomogeneous line caused by statistical variations in the spectral density of absorbers in each frequency interval. In this work, a model and an analysis of statistical fine structure using autocorrelation techniques are presented, and the dependence of the effect for pentacene in p-terphenyl at 1.4K on modulating frequency, detection phase, sample position, center concentration, and site is described. Statistical fine structure provides a new method for probing inhomogeneous systems that allows investigation of the underlying probability distribution and the determination of the homogenous linewidth. The fine structure also represents a fundamental limit on the detectability of shallow spectral features in inhomogeneously broadened lines.

20 DISTRIBUTION / AVAILABILITY OF ABSTRACT	21 ABSTRACT SECURITY CLASSIFICATION
☒ UNCLASSIFIED/UNLIMITED ☐ SAME AS RPT ☐ DTIC USERS	unclassified

22a. NAME OF RESPONSIBLE INDIVIDUAL	22b TELEPHONE (Include Area Code)	22c OFFICE SYMBOL
Dr. W. E. Moerner	408-927-2426	

DD FORM 1473, 84 MAR   83 APR edition may be used until exhausted   SECURITY CLASSIFICATION OF THIS PAGE

All other editions are obsolete   unclassified

STATISTICAL FINE STRUCTURE IN THE
INHOMOGENEOUSLY BROADENED ELECTRONIC ORIGIN
OF PENTACENE IN p-TERPHENYL

T. P. Carter[*], M. Manavi[†], and W. E. Moerner

IBM Almaden Research Center

San Jose, California 95120

ABSTRACT: Recently, the first observation of statistical fine structure on an inhomogeneously broadened absorption profile was reported [W. E. Moerner and T. P. Carter, Phys. Rev. Lett. **59**, 2705 (1987)] for mixed crystals of pentacene in p-terphenyl using laser frequency-modulation spectroscopy. Statistical fine structure is time-independent structure on the inhomogeneous line caused by statistical variations in the spectral density of absorbers in each frequency interval. In this work, a model and an analysis of statistical fine structure using autocorrelation techniques are presented, and the dependence of the effect for pentacene in p-terphenyl at 1.4 K on modulating frequency, detection phase, center concentration, and position in the sample is described. Statistical fine structure provides a new method for probing inhomogeneous systems that allows investigation of the underlying probability distribution function and the determination of the homogeneous linewidth. This fine structure also represents a fundamental limit on the detectability of shallow spectral features in inhomogeneously broadened lines.

[*]IBM Visiting Scientist

[†]Present address: Verbatim Corporation, 435 India Way

Sunnyvale CA 94086

I. Introduction

Inhomogeneous broadening[1] (IB) of atomic or molecular transitions occurs when the individual absorbers in a collection possess homogeneous linewidths which are narrower than the overall lineshape of the collection as a whole, due to a distribution of individual center frequencies. IB is a common feature of the low-temperature spectra of impurity centers in solids that appears in optical spectroscopy[2] as well as in nmr, esr, and Mössbauer experiments.[3] For zero-phonon electronic transitions of crystal impurities, the inhomogeneous distribution (for a particular impurity orientation or site) is a result of any of a variety of imperfections in the host crystal such as dislocations, point defects, or random internal electric fields and field gradients. In amorphous hosts, it is principally the large multiplicity of available sites that leads to IB.

IB is often regarded as an obstacle to the determination of the underlying homogeneous width, which is a fundamental property of the impurity-host combination at a given temperature. Several powerful spectroscopic methods[4] have been developed to extract this information from inhomogeneous systems, including persistent[5] and transient hole-burning as well as such coherent transient techniques[6] as photon-echo, optical free-induction decay and optical nutation. Each of these methods has its strengths and weaknesses; for example, not all systems exhibit persistent hole-burning, and some that do are complicated by spectral diffusion mechanisms which prevent the direct determination of the homogeneous width. If hole-burning does occur, the coherent transient techniques may not be applicable because the high peak intensities normally required in these experiments lead to rapid hole-burning and loss of signal. However, IB is not always regarded in a negative sense: its existence is fundamental to the successful utilization of possibly important future technologies such as frequency domain optical storage.[7]

Inhomogeneously broadened absorption lines are usually regarded as smooth, Gaussian profiles. Recently,[8] we demonstrated the interesting fact that significant fine structure is a

fundamental property of such lines, i.e. inhomogeneous lines are not smooth Gaussian functions if examined closely. The variations from the Gaussian shape of the overall absorption coefficient observed in a given frequency interval Δv are due to statistical changes (number fluctuations) in the absorber spectral density over Δv . The term "statistical fine structure" (SFS) has been coined to refer to this static, time-independent, frequency-dependent structure. It has been shown [8] that SFS can be detected in a *high* concentration sample by using a zero-background technique, namely laser frequency-modulation (FM) spectroscopy. [9] In this work we will describe the theoretical and experimental properties of SFS at a fixed temperature, 1.4 K. We show how the value of the underlying homogeneous linewidth and information about the probability distribution of center frequencies can be derived from the SFS spectra using autocorrelation analysis, a procedure which is fundamentally different from hole-burning or coherent transient techniques.

II. Theory of Statistical Fine Structure in Inhomogeneously Broadened Lines

A. Central Concepts and Definitions

The appearance of statistical fine structure on spectral lines is intimately connected with the microscopic interactions responsible for IB. It is generally accepted that localized perturbations in the vicinity of each absorbing center such as random strains, electric fields, and other perturbations due to defects in the host matrix [3] are responsible for the appearance of IB. In a reasonable approximation these perturbations shift and/or split the absorption line for each center without introducing specific broadening. Thus it is the distribution of center frequencies of absorption that controls the actual shape of the inhomogeneous line.

Each center in the probed volume is assumed to contribute a single Lorentzian profile to the total absorption coefficient. Let $I_\gamma(v) = (\gamma/2\pi)/[v^2 + (\gamma/2)^2]$ signify a single (normalized)

Lorentzian absorption of homogeneous linewidth γ, the full width at half-maximum (FWHM). We restrict without loss of the essential physics to the case of IB for a single site, using the standard definition of a single site as a well-defined orientation of the absorber in the host matrix. If a given center in the site acquires a center frequency of absorption v_o due to the perturbing fields in its vicinity, its absorption function is $L_\gamma(v - v_o)$. The final shape of the complete inhomogeneous line profile is due to the way in which the various absorbers take on specific center frequencies for absorption according to the microscopic values of the local perturbing fields. To be precise, we define the spectral density of absorbers in a fixed probe volume $G(v)$ by requiring that $G(v)dv$ be the number of absorbers with center frequencies in the small interval dv at v. In previous work, $G(v)$ has generally been assumed to be a smooth Gaussian function with FWHM Γ , usually called the inhomogeneous linewidth. In many IB lines, the ratio Γ/γ can be 10^3 or more. In this paper, we examine the implications of our recent experiments showing that $G(v)$ in fact contains significant, fundamental fine structure.

The total (inhomogeneously broadened) absorption coefficient may be written

$$\alpha(v) = s \int_{-\infty}^{+\infty} G(x) L_\gamma(v - x) dx \equiv s \, [G * L_\gamma](v), \tag{1}$$

where s is the integrated absorption strength per molecule and the asterisk signifies convolution. We define the average number of centers per homogeneous linewidth, $\overline{N}_H$, by $\overline{N}_H = < \int_{(\gamma)} G(v) dv >$, where the integration is performed over the homogeneous linewidth γ and the brackets mean to compute the expectation value, i.e., the average value of the integral over many equivalent spectral ranges of width γ . $\overline{N}_H$ is often useful for estimating purposes because spectral structure on $G(v)$ much narrower than γ cannot be deduced from measurements of $\alpha(v)$ due to the convolution operation in Eqn. (1).

In this paper, the various absorbing centers in the sample volume are assumed to be independent and isolated. When $\overline{N}_H \simeq 1$, it is fairly obvious that fine structure would be clearly evident on $\alpha(v)$. However, this paper is primarily concerned with situations in which $\overline{N}_H \gg 1$ so that the total absorption at each frequency in the inhomogeneous line is due to the superposition of many absorbing centers. We will show that even in this "high concentration, but still isolated center" regime, significant, detectable SFS remains and does not average away.

The fine structure on the spectral density $G(v)$ may arise from one of two sources: the presence of special center frequencies that are more probable ("microsites") or from fundamental statistical variations in the total absorption due simply to random selection and superposition (sometimes called number fluctuations). To quantify this, we define the probability distribution function (pdf) for center frequencies, $p(v)$, by requiring that $p(v)dv$ be the probability that a randomly selected absorber in the fixed probe volume will have center frequency in the range dv at v. This pdf is a direct result of the large variety of local environments and center frequencies that are accessible to a randomly chosen center in the probe volume. We distinguish two possibilities as shown schematically in Figure 1. In case (a), $p(v)$ is a smooth Gaussian profile indicative of a normally-distributed set of local perturbations for the single site. In case (b), $p(v)$ contains departures from the normal distribution implying that certain center frequencies are more probable than others due to the presence of special defects or "microsites". This portrayal of $p(v)$ for microsites is only schematic in that the actual departures from a Gaussian function could be either broader or narrower than shown in the figure.

A central goal of this paper is to determine whether our observations of SFS give support to one or the other form for $p(v)$ shown in Figure 1. In doing so, it is important to realize that the *actual* absorber spectral density $G(v)$ measured for a fixed probe volume is just a statistical sample of the underlying pdf, $p(v)$. This means that if the absorbing centers could

be removed from the host and re-doped into the sample many times, the resulting $G(v)$ functions measured for the same volume from the various samples would give information about the form of $p(v)$.

B. Scaling of Statistical Fine Structure

It is instructive to simulate the form of the fine structure that would be expected due to statistics alone for $p(v)$ given by Fig. 1(a). Consider a fixed frequency interval Δv within the inhomogeneous line that satisfies $\Gamma \gg \Delta v \gg \gamma$. On the interval Δv, $p(v)$ would be constant and frequency independent. Since the various absorbing centers are independent and isolated, a uniform random number generator can be used to select center frequencies v_0, and the total absorbance can be generated by adding corresponding Lorentzian functions $L_y(v - v_0)$. Figure 2, trace (a), shows a simulated $\alpha(v)$ for only two absorbing centers each with $\gamma = 0.1\Delta v$ corresponding to $\overline{N}_{II} = 0.2$.

Traces 2(b)-(e) show a simulation of $\alpha(v)$ for $\overline{N}_{II} = 1$, 10, 100, and 10^4, respectively. Let $\Delta\alpha$ and $\overline{\alpha}$ signify the rms amplitude and mean value of α on the interval Δv. The figure shows that $\overline{\alpha}$ grows linearly with $\overline{N}_{II}$, while the relative rms deviations $\Delta\alpha/\overline{\alpha}$ fall approximately as $(\overline{N}_{II})^{-1/2}$. This is reminiscent of the well-known result from statistical physics [10] that the relative fluctuation of an additive physical quantity over statistically independent systems falls as the inverse square root of the number of systems.

To see this more precisely, allow the interval Δv to be divided up into smaller intervals of width γ and compute $N_{II} = \int_{(\gamma)} G(v)dv$ for each interval. Since the various intervals are approximately independent and the overall pdf is uniform, the values of N_{II} can be viewed as successive samples of an additive random variable; hence $(\Delta N_{II})/\overline{N}_{II} \cong (\overline{N}_{II})^{-1/2}$ where ΔN_{II} is the rms fluctuation of N_{II}. Since on each interval the absorption coefficient is directly proportional to the number of centers, we conclude that $\Delta\alpha/\overline{\alpha} = (\Delta N_{II})/\overline{N}_{II} \cong (\overline{N}_{II})^{-1/2}$. Since these deviations of the absorption coefficient from its

average value follow only from the statistics of formation of the line, we call the resulting frequency-dependent deviations "statistical fine structure".

Methods of detecting SFS that are sensitive to the *overall* absorption such as fluorescence and transmission spectroscopy would find the largest relative fluctuations at small $\overline{N}_H$. However, detecting a very small number of centers in the presence of interfering background from the host matrix is very difficult. [11] On the other hand, if detection techniques are used that measure only $\Delta\alpha$, i.e., the deviations of α from its average value, the signal would *grow* as $(\overline{N}_H)^{1/2}$, and easy-to-manufacture *high* concentration samples would yield more easily detectable SFS (as long as the concentration is not so large that no light reaches the detector). To show that the absolute signal in the $\overline{N}_H \gg 1$ regime is clearly larger, Figure 1(f) shows the absorption coefficient of 1(e) with the background subtracted. The peak-to-peak variations in α are 1,600 units compared to only 6 units for trace 1(a).

Assuming that a zero-background detection technique is used that measures only $(\Delta\alpha)l$ where l is the sample length, one may easily compute the dependence of the signal on the sample dimensions and center concentration:

$$(\Delta\alpha)l \sim \sigma(\overline{N}_H)^{1/2}/\Lambda = \sigma(\rho l/\Lambda)^{1/2}, \qquad (2)$$

where σ is the peak absorption cross section per center, Λ is the beam area, and the volume density per homogeneous linewidth is $\rho = \overline{N}_H/\Lambda l$. Therefore, $(\Delta\alpha)l$ and hence the SFS signal increase if the concentration of absorbers or the sample length increases, and increase for smaller laser spots. Further, centers with higher cross section lead to larger SFS signals.

For a given beam area, the maximum signal occurs when the sample length l is equal to the Rayleigh range. In this limit, $(\Delta\alpha)l = \sigma(2\rho/\lambda)^{1/2}$, where λ is the the optical wavelength, and the signal is independent of the focal diameter. In this regime, the probing intensity can be decreased without loss of signal by choosing a larger beam area and a correspondingly longer sample. Of course, an ideal sample geometry for detection of SFS would be a doped

optical fiber in which a small focused spot can be maintained over an arbitrarily long distance. For more conventional samples, the sample length is limited, and small values of Λ are required to observe SFS.

C. Detection Using Laser FM Spectroscopy

In this paper, SFS on $\alpha(v)$ will be detected using laser FM spectroscopy.[9, 12] The specific experimental apparatus will be described in Section III; here we only describe how the use of this technique enables us to detect the structure on $\alpha(v)$. In FM spectroscopy, a phase-modulated light beam consisting of a carrier at the laser frequency v and two sidebands at $(v + v_m)$ and $(v - v_m)$ is generated by passing the laser beam through an electro-optic phase modulator driven at v_m. The modulating frequency v_m is chosen to be larger than several MHz, so that detection may be performed at frequencies where the laser noise consists essentially only of quantum shot noise.[13] Such a phase-modulated light beam contains no amplitude modulation as long as residual AM effects[14] are not present. The phase-modulated beam passes through the sample, and amplitude modulation then appears whenever the amplitudes and/or phases of the two sidebands are disturbed by a frequency-dependent spectral feature in the sample. A high-speed detector and phase-sensitive electronics are used to detect any amplitude modulation on the transmitted beam. If there is no spectral feature present, the photocurrent is not modulated; thus the FM signals appear on zero background.

A crucial feature of the FM technique is that by simple adjustment of an electronic phase shifter, detection may be performed in either quadrature with respect to the modulating signal. Adjustment of the detection phase controls whether the detected signal is proportional to the absorptive or the dispersive effects of the underlying spectral feature. The detected signal varying as $\cos(2\pi v_m t)$, $F_1(v)$, is proportional to

$$F_1(v) \sim - MP_0 e^{-\alpha_0 l} [\alpha(v + v_m) - \alpha(v - v_m)]l, \tag{3}$$

where P_o is the laser power on the sample, M is the modulation index measuring the strength of the sidebands relative to the carrier, l is the sample length, and α_o is the background value of α. This expression is strictly correct in the limit of small M; higher order expressions exist[15] but are not important for the purposes of this paper. Thus the cosine phase signal $F_1(v)$ measures the difference in αl at the two sideband frequencies, as long as $\alpha_o l$ is not too large (i.e., as long as the exponential factor in Eqn. (3) is near unity).

The component of the detected photocurrent varying as $\sin(2\pi v_m t)$, $F_2(v)$, is proportional to

$$F_2(v) \sim MP_o \, e^{-\alpha_o l} \left[\phi(v + v_m) + \phi(v - v_m) - 2\phi(v) \right], \tag{4}$$

where $\phi(v) = n(v)l/(2\pi v/c)$, $n(v)$ is the index of refraction, and c is the speed of light. Thus, F_2 measures the second difference of the frequency-dependent index of refraction at the frequency of the carrier and the two sidebands, as long as $\alpha_o l < 1$.

For either choice of phase, the detected FM signal approaches one of two well-defined limits depending upon the size of the modulating frequency v_m compared to the width of the spectral feature. When $v_m > \gamma$, it is easy to see that only one sideband or the carrier interacts with the spectral feature at a time. Figure 3(a) and (b) shows the resulting FM signals for a single Lorentzian profile L_y in both phases. In the cosine phase (Fig. 3(a)), the FM signal consists of a pair of copies of the original $L_y(v)$, one positive and one negative, separated by $2v_m$. In the sine phase (Fig. 3(b)), three copies of the dispersion due to $L_y(v)$ are generated as shown, spaced by v_m. Further, when the modulating frequency is much larger than γ, the FM signals have an amplitude that is independent of the value of v_m. In the opposite limit of small modulating frequency, traces 3(c) and 3(d) show that for either phase the resulting FM signals approach the derivative of the Lorentzian, and in fact the amplitude of the signals goes to zero linearly with v_m. More examples of FM lineshapes for intermediate values of v_m/γ are shown in Ref. (12).

Since the largest FM signals occur for $v_m \gg \gamma$, this regime of FM spectroscopy was used whenever possible to detect SFS. One may think of Eqns. (3) and (4) as defining an "FM transformation" that is applied to the total absorption in Eqn. (1).

D. Autocorrelation of SFS Spectra

Estimates of the homogeneous linewidth γ can be extracted from the FM-detected SFS spectra by exploiting the properties of autocorrelation functions. This occurs because the total SFS signal is a linear superposition of many single Lorentzian FM spectra with different center frequencies. In a sense, the autocorrelation operation removes the information about the individual center frequencies in order to reveal the underlying homogeneous width. Consider the autocorrelation of Eqn. (1):

$$[\alpha \star \alpha](v) \equiv \int_{-\infty}^{+\infty} \alpha(v')\alpha(v' + v)dv', \tag{5}$$

where the star signifies correlation as distinct from convolution. A useful identity[16] for arbitrary functions f, g, h, and j is

$$(f * g) \star (h * j) \equiv (f \star h) * (g \star j). \tag{6}$$

Further, the autocorrelation of a Lorentzian with itself is another Lorentzian of twice the width:

$$[L_\gamma \star L_\gamma](v) = L_{2\gamma}(v). \tag{7}$$

The result of applying these relations to Eqn. (5) is

$$[\alpha \star \alpha](v) = s^2 [(G \star G) * L_{2\gamma}](v). \tag{8}$$

Since the absorber spectral density G can contain frequency-dependent structure, the autocorrelation G★G is not simple in general. Progress can be made, however, by considering the expectation value of Eqn. (8),

$$< \alpha \star \alpha > (v) = s^2 [< G \star G > * L_{2\gamma}](v), \qquad (9)$$

where the expectation value is taken over many spectra $\alpha(v)$ derived from the same pdf. Under the crucial assumption that the pdf is uniform (Figure 1(a)), $< G \star G >$ approaches the autocorrelation of a broad Gaussian function. The result near $v = 0$ is

$$< \alpha \star \alpha > (v) \sim s^2 L_{2\gamma}(v) + (\text{ terms much wider than } \gamma), \qquad (10)$$

which near the origin is a single Lorentzian profile with FWHM equal to 2γ .

Equation (10) applies for the actual absorption, whereas the measured SFS spectra are related to $\alpha(v)$ by the FM transformation, Eqns. (3) or (4). It would be ideal to apply an "inverse FM transform" to the FM data in order to study the actual shape of $\alpha(v)$. Such a transformation can be derived by Fourier techniques for the cosine phase with the result

$$\alpha(v) \sim \mathscr{F}^{-1}[F_1(y)/2i \sin(2\pi v_m y)], \qquad (11)$$

where $\mathscr{F}^{-1}$ stands for the inverse Fourier transform and $F_1(y) = \mathscr{F}[F_1(v)]$. Unfortunately, Eqn. (11) is difficult to compute for actual SFS spectra acquired over a limited spectral range Δv due to the lack of knowledge of $\alpha(v)$ on the boundaries of Δv and the presence of multiple poles in the inverse Fourier transform.

Since it is a nontrivial problem to invert the FM operation for SFS spectra, we next consider the autocorrelation of the FM cosine phase signal, $[F_1 \star F_1](v)$. We further restrict to the large modulating frequency regime $v_m \gg \gamma$, although similar results can also be derived for the opposite limit. For $c^{\tau_0 l} \sim 1$, the SFS FM signal can be written

$$F_1(v) \sim s \, G \, * \, [L_\gamma(v + v_m) - L_\gamma(v - v_m)], \tag{12}$$

where in this equation and where necessary below we depart from rigor in the notation in order to explicitly display the center frequencies of the Lorentzian functions. Using the fact that

$$L_\gamma(v - v_m) \star L_\gamma(v + v_m) \equiv \int_{-\infty}^{+\infty} L_\gamma(v' - v_m) L_\gamma(v' + v_m + v) dv' = L_{2\gamma}(v + 2v_m), \tag{13}$$

the result is

$$[F_1 \star F_1](v) = s^2 \, (G \star G) \, * \, [- L_{2\gamma}(v + 2v_m) + 2L_{2\gamma}(v) - L_{2\gamma}(v - 2v_m)]. \tag{14}$$

The right-hand side of the convolution operation will be recognized as the autocorrelation of F_1 for a single, isolated Lorentzian absorption. The bracketed expression is schematically shown in Figure 4(a) for positive frequencies only. In this and in other figures, we usually plot the normalized form of Eqn. (5) for convenience.

As was the case for $\alpha \star \alpha$, it is useful to take the expectation value of the autocorrelated SFS FM signal in order to simplify the influence of $G \star G$. Under the assumption of no structure on $p(v)$ over spectral ranges narrower than v_m, the function $< G \star G >$ is relatively constant over the range of the convolution where the bracketed term is large, leaving

$$< F_1 \star F_1 > (v) \sim [- L_{2\gamma}(v + 2v_m) + 2L_{2\gamma}(v) - L_{2\gamma}(v - 2v_m)] \tag{15}$$

as the dominant form near the origin $v = 0$. Thus an estimate for γ can be derived from the FWHM or, more reliably, from the second derivative of $< F_1 \star F_1 >$ at the origin. In words, the expectation value of the autocorrelation of the F_1 signal has a FWHM equal to twice

that for the underlying homogeneous absorption lines. The approximations made are most correct near $v = 0$, so a reasonable formula for the homogeneous width is

$$\gamma \simeq \left[-2 \frac{<F_1 \star F_1 >(0)}{<F_1 \star F_1 >''(0)} \right]^{1/2}, \tag{16}$$

where the double prime signifies second derivative.

For the dispersion signal present in the sine phase, we define the normalized index change for a single isolated Lorentzian at the origin by

$$D_\gamma(v) = \frac{-v/\pi}{v^2 + (\gamma/2)^2} . \tag{17}$$

This function also has the useful property that

$$[D_\gamma \star D_\gamma](v) = L_{2\gamma}(v). \tag{18}$$

For the complete inhomogeneous line the phase shift is then

$$\phi(v) = sk_0 l \, [G \ast D_\gamma](v), \tag{19}$$

where k_0 is the wavevector at line center. Using the expression for the FM signal in the sine phase (Eqn. 4) and an analysis similar to that for F_1, we find

$$<F_2 \star F_2 >(v) \sim [L_{2\gamma}(v + 2v_m) - 4L_{2\gamma}(v + v_m) + 6L_{2\gamma}(v) - 4L_{2\gamma}(v - v_m) + L_{2\gamma}(v - 2v_m)]. \tag{20}$$

The positive frequency portion of the bracketed expression is shown in Figure 4(b), which is simply the autocorrelation function of the F_2 spectrum for a single Lorentzian as shown in Figure 3(b).

In some experiments, it is necessary to consider the case where the modulating frequency is much less than the homogeneous width. In this case for either detection phase, the FM signal is composed of a superposition of the first derivative of many Lorentzian profiles with randomly located center frequencies. The expected autocorrelation of the FM signals may be computed by taking the $v_m < \gamma$ limit of Eqn. (14):

$$< F \star F > (v) \sim \frac{-s^2 \gamma}{\pi} \left[\frac{3v^2 - \gamma^2}{(v^2 - \gamma^2)^3} \right], \tag{21}$$

where F stands for either F_1 or F_2.

Since the size of the FM signals depends upon the ratio γ/v_m, it may also be possible to determine the homogeneous width by measuring the dependence of the rms value of the SFS spectra on modulating frequency. By inspection of the definition of the autocorrelation function, the mean square value of a FM spectrum is equal to the value of the (unnormalized) autocorrelation function at $v = 0$. Using Eqn. (15), then

$$\text{rms}[F_1(v)] \sim 2 \left(\frac{2}{\pi \gamma} \right)^{1/2} \frac{v_m}{(4v_m^2 + \gamma^2)^{1/2}} \ . \tag{22}$$

The value of γ could then be determined by fitting experimental data to this functional form. This method for determining γ will be examined in Section IV along with the method arising from Eqn. (16).

III. Experimental

The low temperature electronic absorption spectrum of pentacene in single crystals of p-terphenyl has been studied in detail.[17, 18] At low concentrations, pentacene exhibits four $S_1 \leftarrow S_0$ site origins of virtually identical intensity, width and shape, corresponding to four inequivalent orientations of pentacene in the low temperature p-terphenyl lattice. These

pentacene origin lines will be referred to as O_1 -O_4, with increasing index denoting increasing center frequency value. The absorption line for each site has an overall Gaussian profile indicative of inhomogeneous broadening, with a $\Gamma \simeq 40$ cm^{-1}. In previous photon-echo studies, the homogeneous linewidth y at 1.4 K for all sites has been measured and been shown to be determined solely by the radiative lifetime, with values of 7.8, 7.3, 18.1 and 18.5 MHz for O_1 -O_4, respectively. [19]

Samples of pentacene in *p*-terphenyl were prepared from twice sublimed pentacene and extensively zone-refined *p*-terphenyl. Dilute single crystals were grown using the Bridgman method. Polycrystalline samples were made by placing a small amount of powdered pentacene/*p*-terphenyl mixture between glass cover slips and heating on a hotplate at $\sim$ 200° C until molten, then allowing them to cool fairly rapidly. Pentacene concentrations ranged from 1×10^{-5} to 2×10^{-7} mole/mole, which are within the regime where the molecules may be regarded as isolated absorbers. [20] Sample thicknesses ranged from 10-20 μm for polycrystalline samples and 250-400 μm for single crystals, yielding low temperature peak optical densities between 0.01 and 0.15 for the pentacene O_1 line. [17]

SFS spectra were acquired using the experimental apparatus shown in Figure 5. Light from a single-frequency, actively stabilized, tunable CW dye laser DL (Coherent 599-21, jitter linewidth $\simeq 2.8$ MHz) was first passed through an amplitude stabilizer AS (Cambridge Research LS-100) to reduce laser intensity fluctuations, and then frequency-modulated by an electro-optic phase modulator EO (AD*P, Lasermetrics 1239C). The modulated beam was reflected off the input mirror of a confocal Fabry-Perot etalon FP (Tropel 240, either 1.5 GHz or 7.5 GHz FSR). When the etalon was tuned so that the laser scanned over the dip in reflectance due to the etalon fringe, a large FM signal was produced which was used as a standard for measuring detection sensitivity and for adjustment of the rf phase. For acquisition of SFS spectra, the etalon spacing was adjusted so that no resonance fringe

occurred in the laser scan range and for this reason, scans were limited to a range less than the FSR of the etalon. The laser was typically set to scan at its maximum rate, 0.25 s/scan.

The laser intensity was selected using a combination of fixed and variable neutral density attenuators VA, and then focused on the sample S using a 100 mm focal length achromatic doublet lens to a spot $\simeq 20 \ \mu m$ in diameter. The total laser power on the sample was approximately 5 μW, adjusted to compensate for sample absorption, scattering, and cryostat losses in order to maintain 1.5 μW at the detector. The transmitted light was collected and focused onto the detector PD (a Si avalanche photodiode, either Analog Modules LNOR-275MHz-15kV/A or an RCA C30950F with integral preamplifier). The detector output was amplified by A_1 (Q-Bit 538, 34 dB) and sent to the rf port of a double-balanced rf mixer M (Mini-Circuits ZFM-3H). The rf modulation frequency was provided by a precision rf signal generator O (Marconi Instruments 2019A) whose output was split by a two-way, 0° power splitter PS (Mini-Circuits ZFSC-2-5). One splitter output port was used to drive the local oscillator port of the mixer; the other output port was amplified by A_2 (ENI 503L, 40 dB) in series with A_3 (Hewlett-Packard 230B) and used to drive the electro-optic modulator, typically with 30 V rms across a 50 Ω load. This provided a modulation index $M \sim 0.3$. Adjustment of the rf phase of the detector output at the mixer was accomplished by slightly detuning the center frequency of A_3. In this way, the FM transform of either the absorbance (F_1) or dispersion (F_2) of an SFS spectrum could be obtained. The mixer IF output was amplified by PMPA (a low-noise post-mixer pre-amplifier,[21] dc-20 kHz) and band-pass filtered by BPF (Tektronix 7A22 differential amplifier in a 7904 oscilloscope, bandpass -3dB points 1 Hz - 300 Hz, typically) before being digitized and averaged by DS (either a Tektronix 468 oscilloscope, a LeCroy 3500SA transient digitizer or a Data Precision Data 6000 waveform analyzer).

It should be kept in mind throughout this work that, unless specifically noted, no significance should be placed on the absolute intensities of the SFS signals since the detector

and overall amplification varied from one experiment to another in order to maximize the signal-to-noise. This does not in any way affect the conclusions which are made herein.

IV. Results and Discussion

As previously stated, SFS is a static, time-independent property of inhomogeneous absorption lines at low temperatures. This is illustrated for the case of the O_1 line of pentacene in p-terphenyl in Figure 6. The laser center frequency was repetitively scanned over a 2 GHz frequency range, with SFS data acquired during the both the forward and backward scan. In this figure, an FM signal of 1 V corresponds to a value of $(\Delta\alpha)l$ of approximately 10^{-3}. The large peaks at 0 and 2 MHz are end-of-scan artifacts and will be discussed below. The smaller, narrower features between the large peaks are the actual SFS on the O_1 line. The mirror symmetry between the up-scan and down-scan regions of the spectrum is convincing evidence that the SFS peaks are reproducible features in the frequency domain; their static nature is further demonstrated by the similarity of successive averages taken several minutes apart, one of which is shown in Figure 6 offset vertically for clarity.

Figure 6 was obtained using a higher laser power and a smaller M than the values stated in Section III; the high laser power produced the artifacts at 0 and 2 GHz (representing the limits of the scan) which are signatures of a shallow trench caused by weak hole-burning[R] during the scanning of the spectrum. This hole-burning is very inefficient and the saturation hole depth is very small. For the results presented in the rest of this paper, the effect of hole-burning on the SFS spectra was made negligible by reducing the total laser power to 1.5 μW at the detector and increasing the FM modulation index to the maximum value we could achieve with our modulator, $M \sim 0.3$.

Further information about the nature of SFS spectra is depicted in Figure 7, where the bottom panel shows a 5 GHz wide scan of the SFS near the peak of the O_1 line. Broad range SFS spectra like this are easily mistaken for a snapshot of some noisy signal. However, their

static, reproducible nature is demonstrated by the two traces in the top panel of Figure 7, the lower of which is an expansion of the trace in the bottom panel; the upper trace is a subsequent acquisition of the same spectral region more than 20 min later. The agreement is quite good, indicating that at this temperature (1.4 K) there is little or no rearrangement or annealing of the perturbations producing the IB which were "frozen" when the crystal was cooled. Most, if not all, of the slight differences between the spectra are due to the quantum and avalanche noise of the detection system. However, some of the changes in the SFS structure may be induced by the probing process since weak persistent spectral hole-burning does occur. The signal-to-noise ratio (SNR) of these and other averaged spectra of the O_z SFS in this work is $\simeq$ 8-10, measured as the ratio of the rms signal levels when the laser is tuned on and off the pentacene absorption line.

The possibility of spontaneous rearrangement of the SFS structure at low temperature has not been ruled out, however. Preliminary experiments to determine the magnitude of spontaneous rearrangement at slightly higher temperatures were inconclusive due to technical problems associated with the focused geometry needed to observe large SFS signals in thin samples. The slight motion of the sample during temperature cycling prevented reliable measurement of the same sample volume before and after the temperature excursion. We did note however that the SFS spectra obtained at slightly higher temperatures (ca. 4-10 K) were significantly broadened.[8] This is consistent with the published dependence of γ on temperature for this system.[22] Although it is not the purpose of this work to investigate the temperature dependence of γ, SFS can and should be used to do so in future studies.

Laser FM spectroscopy can be used to probe either the absorption or dispersion of a sample, depending on the relative phases of the signals at the local oscillator (L) and rf (R) inputs to the mixer. When these signals are in phase (the F_1 signal, Eqn. (3)) the absorption of the sample is probed; when they are 90° out of phase, a signal dependent on the dispersion of the sample is generated (F_2, Eqn. (4)). Representative spectra taken in the different phases

over same spectral region are shown in Figure 8 for the O_1 line of pentacene. Traces 8(a) and (b) show the F_1 and F_2 signals when $v_m = 150$ MHz, respectively, and traces (c) and (d) are the F_1 and F_2 signals when $v_m = 20$ MHz . Each spectrum was obtained twice to check the reproducibility of the SFS. Note that the "density" of features in the F_2 spectrum in 8(b) is slightly greater than that in 8(a); this occurs because the F_2 transform produces three features from each Lorentzian dispersion feature when v_m/γ is large, while the F_1 transform produces only two features from each Lorentzian absorption line. Otherwise, the F_2 spectra seem quite similar to those taken in F_1 phase. As illustrated in 8(c) and (d), the magnitude of the SFS decreases when v_m decreases because the FM sideband splitting is comparable to the width of the features being probed (see Figure 2(c) and 2(d) for comparison). The detailed dependence of the SFS signals on the value of v_m will be discussed below.

Since the SFS technique probes only a small volume of the sample, it is interesting to investigate how (or if) the SFS structure changes as one moves transversely to different spatial locations. The result of such a study is presented in Figure 9, which shows a portion of the F_2 SFS "landscape" of a fixed frequency region of the O_1 line for a small range of laser spot positions in a single crystal of pentacene in p-terphenyl. The acquisition of these data was accomplished by obtaining 101 F_2 SFS spectra, each in a 20 μm diameter laser spot, and moving the position of the laser beam on the sample by 2 μm along a single spatial axis between spectra. The same data are presented in a different way in Figure 10, where the SFS intensities are represented as various shades of grey in a two-dimensional plot of laser frequency versus laser spot position. Close examination of the data reveals that the features extend over several spot positions, which is merely a reflection of the fact that adjacent spectra were obtained from highly overlapping probe volumes. The important point here is that there are no features which extend over a long range along either the frequency or position dimensions. This is indicative of the absence of microsite structure in the frequency range detectable by the FM modulation frequency used (58.1 MHz). In other words, since the SFS structure changes dramatically and apparently randomly from one sample volume

to another, special frequencies that are more probable than others do not appear to be present.

It is possible to search for underlying correlations in the data of Figs. (9) and (10) by computing autocorrelation functions along both the frequency and space axes. The top panel of Figure 11 shows the average of 101 autocorrelations along the frequency axis, and there is no significant feature in this autocorrelation which is not described by Eqn. (20). The presence of microsite structure would be expected to produce some new feature, not described by the theory presented in Section II. The bottom panel shows the average of 512 autocorrelations along the spatial dimension, one for each frequency in the laser scan. This operation tests whether a large peak at a given frequency has a tendency to reappear at other spatial locations some distance away. The shape of the lower trace approximates a $(\sin x)/x$ function, which is a result of the fact that the SFS structure along the position axis has been smoothed (low-pass filtered) by the laser spot that extends over several spatial positions. The absence of sharp peaks in the lower trace suggests that spatial locations separated by more than the laser spot diameter of 20 μm are uncorrelated. Both these observations give support to the statistical origin for the observed SFS, i.e., there is no evidence to suggest that microsites exist in this material over frequency ranges smaller than approximately 100 MHz.

We have also performed a preliminary examination of the SFS structure of the O_2, O_3 and O_4 site origins of pentacene in p-terphenyl. Figure 12 shows three in-focus 1.4 K spectra: trace (a) is the FM signal acquired at a laser frequency far removed from the pentacene absorption. This noise level represents the quantum noise from the probe beam and the detector avalanche noise at 150 MHz. In particular, the residual electronic noise with no light on the detector is well below this level, and any residual AM from the modulator is also below this level due to the low light powers in use. Trace (b) is the FM SFS signal near the peak of the O_1 line; and trace (c) is the FM SFS spectrum near the peak of the O_3 line. The SFS in the O_3 line is strikingly different, with lower intensity and broader

spectral features than for the O_1 site. Results similar to those obtained from O_3 occur for the O_4 site, while the SFS of the O_2 site mimics that of the O_1 line. Although the measured homogeneous linewidths for O_3 and O_4 are more than twice as large as those for O_1 and O_2,[19] and therefore should produce smaller FM signals for a given modulation frequency, this effect alone does not explain the far smaller amplitude of SFS observed on these sites. The weaker and broader SFS for the two higher sites may also be due in part to the significant increase in the $S_1 \rightarrow T_1$ intersystem crossing (ISC) quantum yields for the O_3 and O_4 sites ($\Phi_{ISC} \simeq 0.6$) , compared to that for the O_1 and O_2 sites ($\Phi_{ISC} \simeq 4 \times 10^{-3}$). [19] This increase in Φ_{ISC}, together with a triplet lifetime of $\simeq 70 \ \mu s$ [23, 24] allows easy transient bleaching of the $S_1 \leftarrow S_0$ transition during probing, thereby significantly reducing the number of centers contributing to the SFS FM signal and reducing the amplitude of the SFS spectrum.

In Section IIB we argued that the rms intensity of the SFS should be proportional to $(\overline{N}_{II})^{1/2}$ (Eqn. (2)). Figure 13 shows the rms amplitude of a large number of O_1 FM SFS spectra versus $\overline{N}_{II}$ for a sequence of seven polycrystalline thin film samples. The samples were all prepared from a single parent concentration of pentacene in p-terphenyl, using different sample thicknesses to adjust $\overline{N}_{II}$. The actual value of $\overline{N}_{II}$ for each sample was determined from the room-temperature optical density, the extinction coefficient ($\varepsilon = 9.9 \times 10^3$) [23] and the low-temperature inhomogeneous broadening factor for these polycrystalline samples, $\Gamma/\gamma = 1.1 \times 10^4$. The straight line is a least-squares fit to the data showing that the rms amplitude of $F_1(v)$ grows as $(\overline{N}_{II})^{0.54 \pm 0.05}$ which is consistent with the expected $(\overline{N}_{II})^{1/2}$ dependence. The vertical scatter in the points is understandable, because each FM spectrum was acquired over a different spectral range.

The rms value of a given SFS spectrum also depends upon the relative sizes of v_m and γ (see Figures 3 and 8) and, in principle, it is possible to determine the underlying homogeneous linewidth of an SFS spectrum by measuring the rms value as a function of

v_m. Figure 14 shows the measured v_m dependence of the in-focus rms SFS signal for the O_1 line using F_1. Each data point (circle) at a particular v_m represents the mean rms value of a set of 11 in-focus O_1 SFS spectra taken at different center frequencies to provide a good statistical sample of the SFS. This method reduces any scatter from the true rms SFS value which might occur for a single spectrum due to local fluctuations of $G(v)$. The error bars represent two times the standard deviation of the set of individual rms values obtained at a given v_m. The same set of center frequencies was used at each new v_m. The data are corrected for modulation-frequency-dependent changes in the detection sensitivity, most notably for changes in the modulation index. The two solid lines in Figure 14 are simulated curves using Eqn. (22): the lower line assumes a value of γ equal to 40 MHz, and the upper line is the analogous simulation using the previously measured value [19] of γ, 7.8 MHz. The non-zero value of the simulations at $v_m = 0$ represents the residual off-line averaged quantum + avalanche noise level of 13 mV. Clearly, the determination of the homogeneous linewidth by this fitting procedure misses the actual value by a large factor.

The departure of the experimental data from the expected 7.8 MHz curve can be explained in the following way. The FM signal from a sample is generated when either of the low intensity FM sidebands is in resonance with some spectral feature. If the intensity of the laser carrier on the sample is above the saturation threshold, power broadening of the homogeneous linewidth and a correspondingly reduced absorbance in the immediate vicinity of the carrier frequency will occur. If v_m is greater than the width of the transient spectral hole formed at the carrier frequency, then both sidebands will be probing an undistorted region of the spectral line, as long as the transient spectral hole from the carrier decays before either sideband can reach the spectral region of reduced absorption. If v_m is comparable to or less than the width of the transient spectral hole formed at the carrier frequency, then both sidebands will probe the broadened features near the carrier. Hence the modulation frequency dependence at low v_m will be dominated by power broadening due to the carrier. From the data presented in Figure 14, we conclude that a power-broadened transient hole

tens of MHz in width has been formed around the carrier frequency. This effect can be minimized by reducing the total laser intensity so that the carrier would no longer saturate the absorption, but this also reduces the SFS signal amplitude proportionally (Eqn. (3)). In principle, this could be compensated for by increasing the modulation index, but in these experiments the electro-optic modulator was always driven at the maximum rf power available (30 V rms into 50 Ω). When the laser power was decreased, the SNR was insufficient to produce good reproducibility.

A much better method of determining γ which does not necessitate the use of low modulation frequencies takes advantage of the properties of autocorrelation functions (see Eqns. (15) and (16)), and has been successfully used on the pentacene/p-terphenyl system. [8] These equations relate to the *expectation* value of $F_1 \star F_1$; the autocorrelation of a single F_1 SFS spectrum does not provide a large enough statistical sample of the SFS structure to yield a reliable approximation for $< F_1 \star F_1 >$ and therefore a reliable value for γ. To illustrate this, normalized autocorrelations of single in-focus, O_1 SFS spectra taken with $\nu_m = 150$ MHz for F_1 and F_2 phases are shown in Figure 15(a) and (b), respectively. Both traces show a large feature at the origin with approximately the correct FWHM (2γ) along with many random fluctuations about the zero level which bear little resemblance to the expected forms of Eqns. (15) and (20). However, if many SFS spectra are obtained over different frequency intervals and their autocorrelations averaged, the expected dependence becomes quite apparent. Traces 15(c) and (d) show the results in the two phases for averages of 66 and 11 spectra, respectively. One can see in these averaged autocorrelations the negative feature predicted at $2\nu_m$ for F_1 as well as the negative feature at ν_m and the positive feature at $2\nu_m$ for F_2 as given in Eqns. 15 and 20. The number of spectra needed to produce an average autocorrelation which approaches the proper expectation value decreases as the frequency range of the scans is widened, because errors in the calculation of the autocorrelation due to the finite spectral range are minimized.

For a single crystal sample with concentration 3×10^{-7} moles/mole, we measure

$\gamma = 7.9 \pm 0.8$ MHz for the O_1 site at 1.4 K by analyzing the autocorrelations of six SFS

spectra using Eqn. (16). The second derivative of the autocorrelation function at the origin

was determined by using a standard five-point central difference formula.[25] Each spectrum

was acquired over a different 4.8 GHz spectral range using $v_m = 150$ MHz. This experimental

value for γ is consistent with the previously reported value[19] of 7.8 ± 0.6 MHz.

Depending upon the experimental conditions, certain artifacts can distort the shape of

the autocorrelation function near the origin and give rise to errors in the determination of

γ using Eqn. (16). It is fairly obvious that errors will occur in the autocorrelation if too few

points are digitized for each spectral range of width γ. If the laser linewidth is not much

smaller than γ, the absorption profile for a single isolated Lorentzian will be the convolution

of a Lorentzian and the laser spectral profile. In addition, if the SNR of the SFS spectrum

is not high enough, a peak at the origin in the autocorrelation due to noise will distort the

value one might determine for the second derivative. Finally, the spectral range over which

the entire SFS spectrum is acquired may be too small to allow approximation of the integral

in Eqn. (5) by a finite sum. The error introduced by each of these in a given experiment

can be estimated by extending the autocorrelation analysis in Section II. In our experiments,

we determined the following useful rules of thumb to keep the error in the use of Eqn. (16)

below a few percent: (i) maintain laser linewidth less than $\gamma/3$, (ii) digitize the SFS spectrum

with at least 5 points per frequency range γ, (iii) choose $v_m > 10\gamma$, and finally (iv) if the

inhomogeneous line is large, acquire spectra over a range of at least $20v_m$ or until the SFS

becomes negligible.

V. Conclusion

Using laser FM spectroscopy, we have observed SFS for the origin lines of the four sites

of pentacene in p-terphenyl crystals, and have presented a formalized theoretical description

of the effect and its analysis. Measurement of the homogeneous linewidth for the O_1 site origin using autocorrelation analysis of SFS spectra yielded a result in excellent agreement with previous determinations. SFS data taken over a range of probe volumes in a single crystal sample to investigate the underlying probability distribution function of the inhomogeneous profile yielded no evidence for the existence of microsite structure on O_1 over frequency ranges smaller than $\simeq 100$ MHz. The dependence of the SFS signals on center concentration, rf modulating frequency and detection phase was measured and found to be in general agreement with the statistical model for the fine structure.

Limitations of the technique may arise from the following facts: (i) the homogeneous linewidth may be so large that high-speed detectors and modulators are not available to achieve the condition for large signals $v_m \gg \gamma$, (ii) persistent spectral hole-burning may prevent the careful detection of SFS due to bleaching by the probing laser, and (iii) the concentration or cross section of the absorber may be too small to yield SFS signals larger than the laser shot noise. Limitation (i) may be overcome by using a variation of FM spectroscopy, the two-tone FM technique,[26] which allows the detection of much broader features with high sensitivity. In spite of the remaining technical limitations, SFS should be a universal property of all inhomogeneously broadened absorption lines, and it is hoped that the techniques described here will be applied to study the low-temperature spectra of other ions and molecules in crystals as well as in amorphous media. If spectra can be acquired in a time short compared to the collision time, SFS may even be observable on the Doppler-broadened profile of a gas. A further interesting question is whether or not SFS can be detected using coherent temporal probes of the inhomogeneous line such as free-induction decay.

It is fairly obvious that SFS is identical in origin to the kind of spectral structure one would expect if the optical absorption due to individual absorbers in a solid could be detected. In more common samples where the number of molecules per homogeneous linewidth is large, statistical fluctuations of the spectral density of absorbers will always occur,

and in these cases SFS not only provides a new window into the sources of inhomogeneous broadening, but the effect also represents a fundamental limit[27] on the detectability of shallow spectral features in solids.

ACKNOWLEDGEMENT

REFERENCES

1. A. M. Portis, Phys. Rev. 91, 1071 (1953).

2. A. L. Schawlow, in *Advances in Quantum Electronics*, proceedings of the Second International Conference on Quantum Electronics, edited by J. R. Singer, (Columbia Univ., New York, 1961), pp. 50-64.

3. A. M. Stoneham, Rev. Mod. Phys. 41, 82 (1969).

4. See *Laser Spectroscopy of Solids*, W. M. Yen and P. M. Selzer, eds., Topics in Applied Physics Vol. 49, (Springer, Berlin, 1981) and references therein.

5. See Persistent Spectral Hole-Burning: Science and Applications, Springer Topics in Current Physics Vol. 44, W. E. Moerner, ed. (Springer, Berlin, Heidelberg, 1988) and references therein.

6. D. A. Wiersma, Adv. Chem. Phys. 47, 421 (1981); J. Hegarty, J. Lum. 36, 273 (1987); R. G. Brewer and R. L. Shoemaker, Phys. Rev. A6, 2001 (1972).

7. W. E. Moerner, J. Mol. Electr. 1, 55 (1985) and references therein.

8. W. E. Moerner and T. P. Carter, Phys. Rev. Lett. 59 , 2705 (1987); W. E. Moerner and T. P. Carter, Bull. Am. Phys. Soc. 32, 1630 (1987).

9. G. C. Bjorklund, Opt. Lett. 5, 15 (1980).

10. L. D. Landau and E. M. Lifshitz, *Statistical Physics, Part 1*, (Pergamon, Oxford, 1980), p. 9.

11. For a description of background problems for liquid hosts, see D. C. Nguyen, R. A. Keller, and M. Trkula, J. Opt. Soc. Am. B 4, 138 (1987).

12. G. C. Bjorklund, M. D. Levenson, W. Lenth, and C. Ortiz, Appl. Phys. B 32, 145 (1983).

13. J. L. Hall, T. Baer, L. Hollberg, and H. G. Robinson, in Laser Spectroscopy V, A. R. W. McKellar, T. Oka, and B. P. Stoicheff, eds. (Springer, Berlin,, 1981), pp. 15-24.

14. E. A. Whittaker, M. Gehrtz, and G. C. Bjorklund, J. Op. Soc. Am. B: Opt. Phys. 2, 1320 (1985).

15. G. Janik, C. Carlisle, and T. F. Gallagher, Appl. Opt. 24, 3318 (1985).

16. See for example R. N. Bracewell, The Fourier Transform and Its Applications, (McGraw-Hill, New York, 1986), p. 328.

17. R. W. Olson and M. D. Fayer, J. Phys. Chem. 84, 2001 (1980).

18. J. H. Meyling and D. A. Wiersma, Chem. Phys. Lett. 20, 383 (1973).

19. F. G. Patterson, H. W. H. Lee, W. L. Wilson, and M. D. Fayer, Chem. Phys. 84, 51 (1984).

20. R. W. Olson, F. G. Patterson, H. W. H. Lee and M. D. Fayer, Chem. Phys. Lett. 79, 403 (1981).

21. D. E. Horne and W. E. Moerner, to be submitted to Rev. Sci. Instr.

22. F. G. Patterson, W. L. Wilson, H. W. H. Lee, and M. D. Fayer, Chem. Phys. Lett. 110, 7 (1984).

23. C. Hellner, L. Lindqvist and P. C. Roberge, Farad. Trans. II 68, 1928 (1972).

24. H. de Vries and D. A. Wiersma, J. Chem. Phys. 70, 5807 (1979).

25. G. A. Korn and T. M. Korn, Mathematical Handbook for Scientists and Engineers, (McGraw-Hill, New York, 1968), p. 737.

26. G. R. Janik, C. B. Carlisle and T. F. Gallagher, J. Opt. Soc. Am. B 3, 1070 (1986).

27. W. E. Moerner, W. Lenth, and G. C. Bjorklund, in Persistent Spectral Hole-Burning: Science and Applications, Springer Topics in Current Physics Vol. 44, W. E. Moerner, ed. (Springer, Berlin, Heidelberg, 1988), pp. 284-285.

FIGURE CAPTIONS

Figure 1. Simulated probability distribution functions. Case (a) is the smooth Gaussian profile usually assumed for an inhomogeneously broadened set of absorbers; case (b) represents a pdf which includes microsites, or departures from the Gaussian form due to certain center frequencies having higher and lower probability than in the normal case.

Figure 2. Simulated absorption spectra. Each spectrum is the sum of single Lorentzians each with $y = 0.1$ and with randomly chosen center frequencies. Traces (a)-(e) correspond to $\overline{N}_{11}$ values of 0.2, 1, 10, 100 and 10^4. The data for trace (f) is the same as that for (e), with the scale expanded about the average value to show the fluctuations still present.

Figure 3. Simulated FM spectra from Eq. (3) and (4). The spectra were generated from a single Lorentzian absorption or dispersion feature centered at 0 MHz with $y = 8$ MHz. Traces (a) and (b) were obtained with $v_m = 150$ MHz ; traces (c) and (d) were obtained with $v_m = 1$ MHz.

Figure 4. Simulated (normalized) autocorrelation spectra. These autocorrelations were calculated from the simulated FM spectra shown in Figure 3(a) and (b).

Figure 5. Experimental apparatus. See text for description of symbols.

Figure 6. SFS of the O_1 line in pentacene in p-terphenyl at 1.4 K. Each trace is the average of 64 scans over a 2 GHz frequency range. The SFS is the smaller, narrower features between the large artifact peaks at 0 and 2 GHz, and shows mirror symmetry in the up and down scan portions of the spectrum. The lower trace is a second acquisition taken several minutes later, offset vertically for clarity.

Figure 7. Wide range scan of SFS. The lower panel shows the result of 64 averages of a 5 GHz scan of the SFS on the O_1 line at 1.4 K. The upper panel shows a portion of the same spectrum on an expanded frequency scale together with another acquisition of the spectrum taken more than twenty minutes later, offset for clarity.

Figure 8. SFS with different detection phases and modulation frequencies. The spectra are the average of 64 scans, all over the same range of frequencies near the peak of the O_1 line at 1.4 K. Traces (a) and (b) are the F_1 and F_2 responses when $v_m = 150$ MHz; traces (c) and (d) are the F_1 and F_2 responses when $v_m = 20$ MHz. Superimposed over each trace is another subsequent average of the spectrum.

Figure 9. Surface plot of SFS spectra at different laser spot positions. Each SFS spectrum is the average of 64 scans over the same range of frequencies. A total of 101 spectra were obtained in the F_2 phase at $v_m = 58.1$ MHz , each with the laser focused to a 20 μm spot on the sample and with the laser spot position displaced by 2 μm along a single spatial axis between spectra.

Figure 10. A 2-dimensional grey scale plot of the same data as that depicted in Figure 9. The shades from white to black indicate the value of the SFS signal, with lighter shades indicating higher values.

Figure 11. Normalized average autocorrelations of the data of Figures 9 and 10 along the two independent axes. The top panel shows the normalized average autocorrelation along the laser frequency axis of all 101 SFS spectra. The bottom panel shows the normalized average autocorrelation along the position axis at 512 discrete laser frequencies.

Figure 12. SFS in the different site origins. Trace (a) is the averaged noise level obtained when the laser is tuned off all absorbance lines; trace (b) is SFS near the peak of the O_1 line, and trace (c) is SFS near the peak of O_3. All spectra were averaged over 64 laser scans in the F_1 phase with $v_m = 150$ MHz and constant detection sensitivity.

Figure 13. Dependence of SFS rms amplitude on $\overline{N}_{II}$. Different $\overline{N}_{II}$ values were obtained by using different thicknesses of sample at the same concentration. The straight line is a least-squares fit to the data, with slope $= 0.54 \pm 0.05$.

Figure 14. Dependence of rms SFS amplitude on v_m. Each circle represents the average of the rms values of 11 F_1 SFS spectra from the O_1 line, each spectrum taken over a different frequency range. The error bars represent $\pm$ two standard deviations for the rms values at that frequency. The two solid lines are simulated curves according to Eqn. (22) using $\gamma = 7.8$ and 40 MHz for the upper and lower curves, respectively.

Figure 15. Normalized autocorrelations in F_1 and F_2. Traces (a) and (b) show the autocorrelations of single F_1 and F_2 O_1 SFS spectra, respectively. Traces (c) and (d) are the averaged autocorrelations of 66 and 11 SFS spectra, respectively, in the two detection phases. All spectra were obtained near the peak of the O_1 line with $v_m = 150$ MHz.
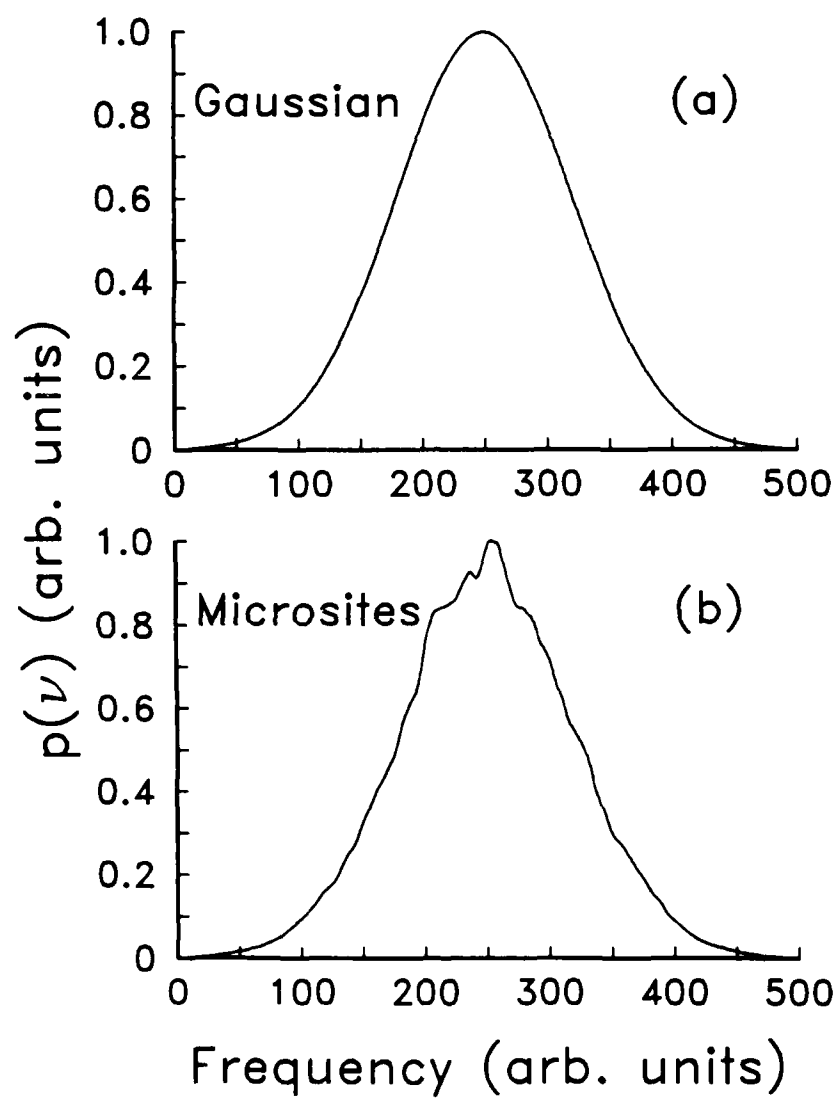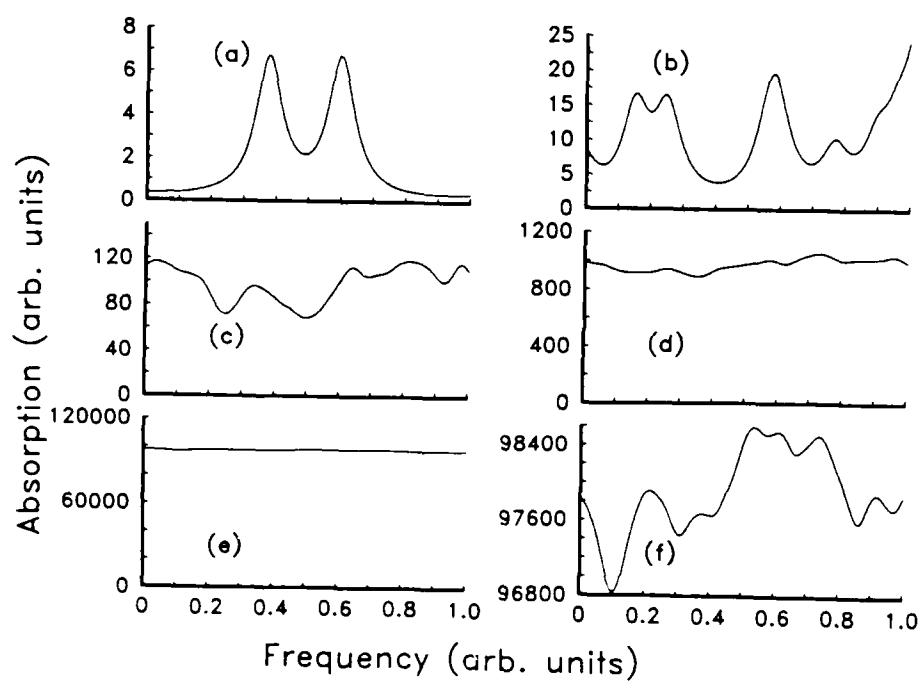
Figure 1
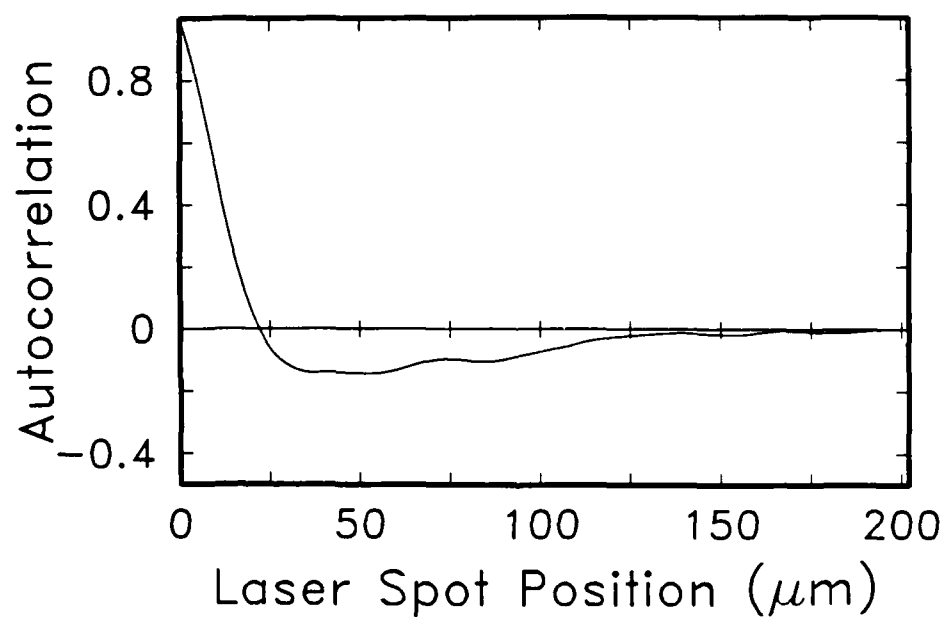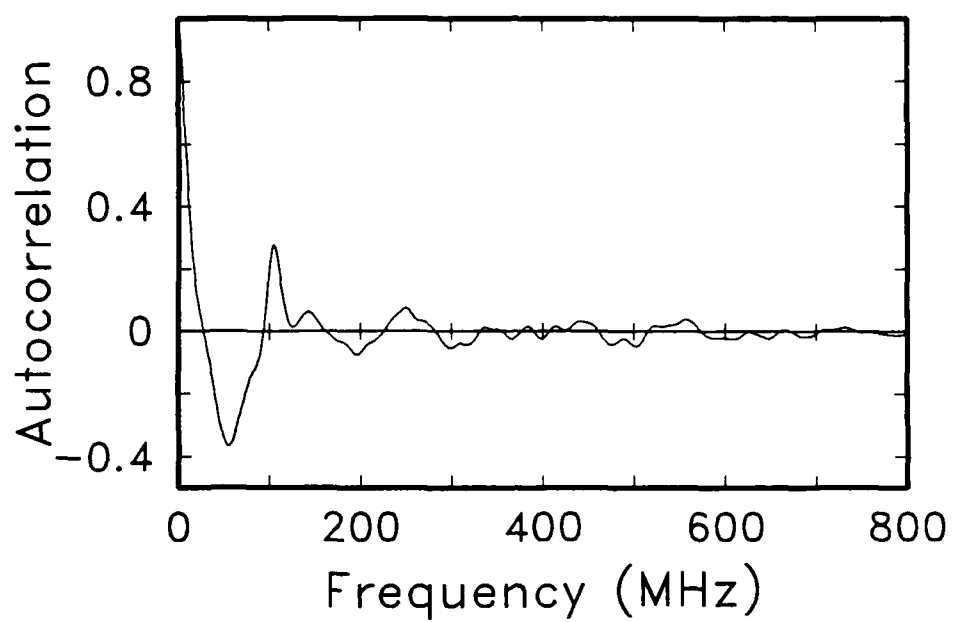
Figure 2
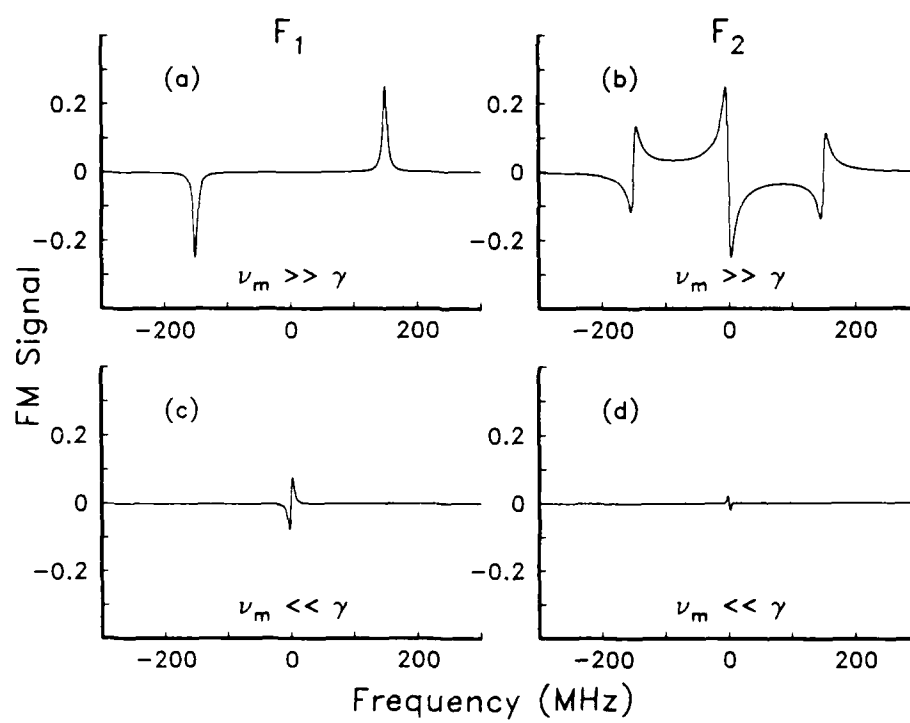
Figure 3
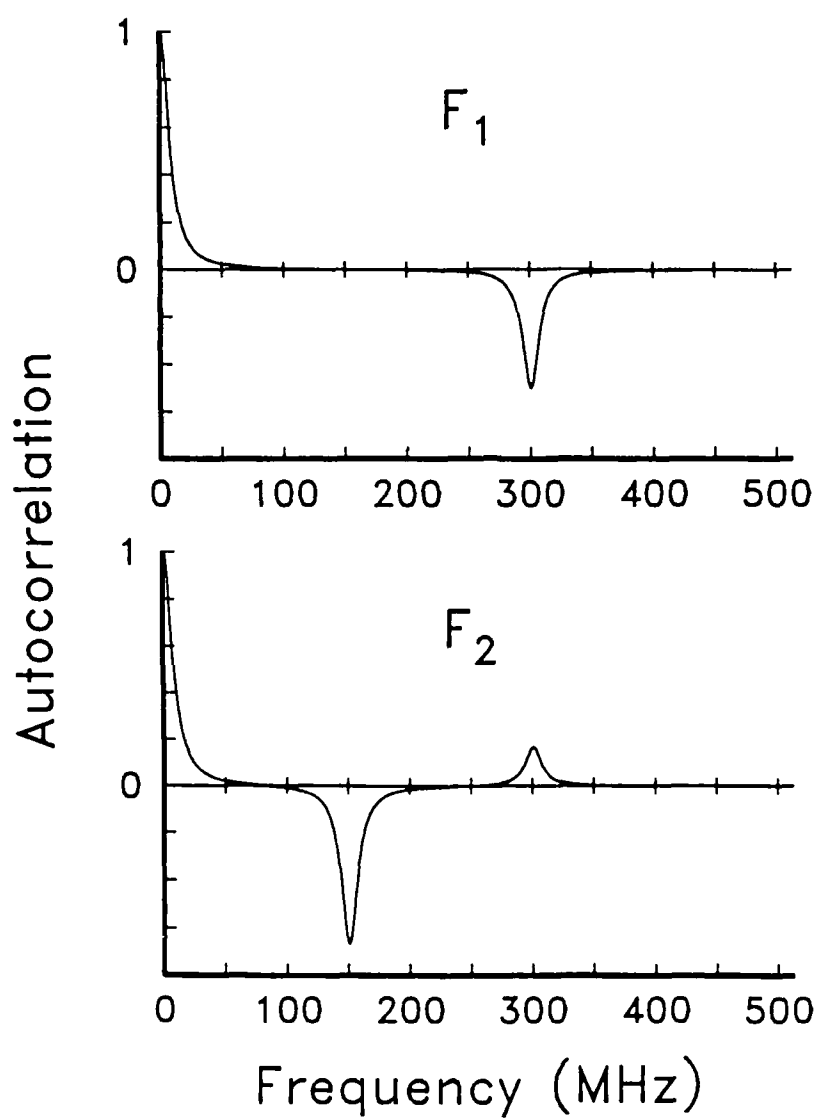
Figure 4
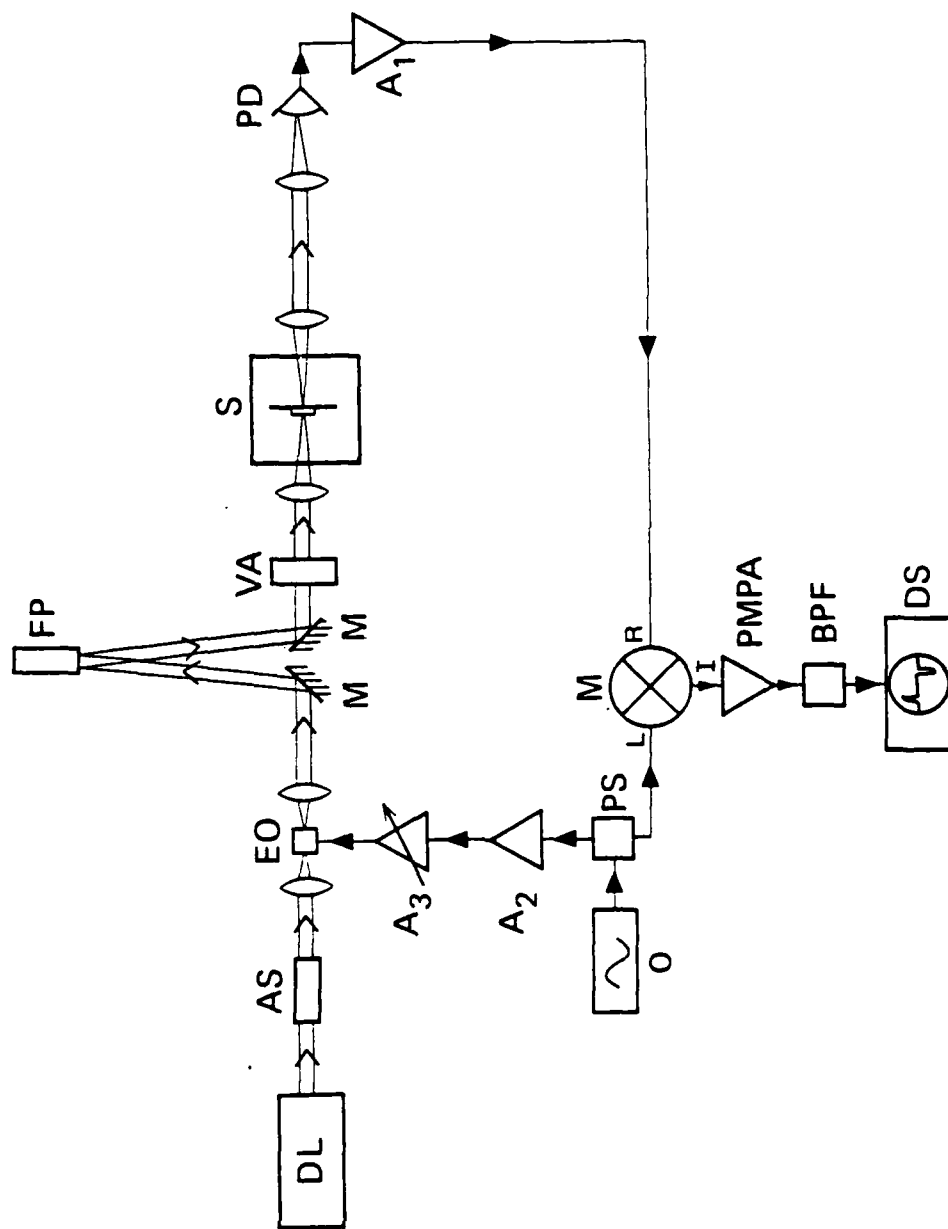
Figure 5
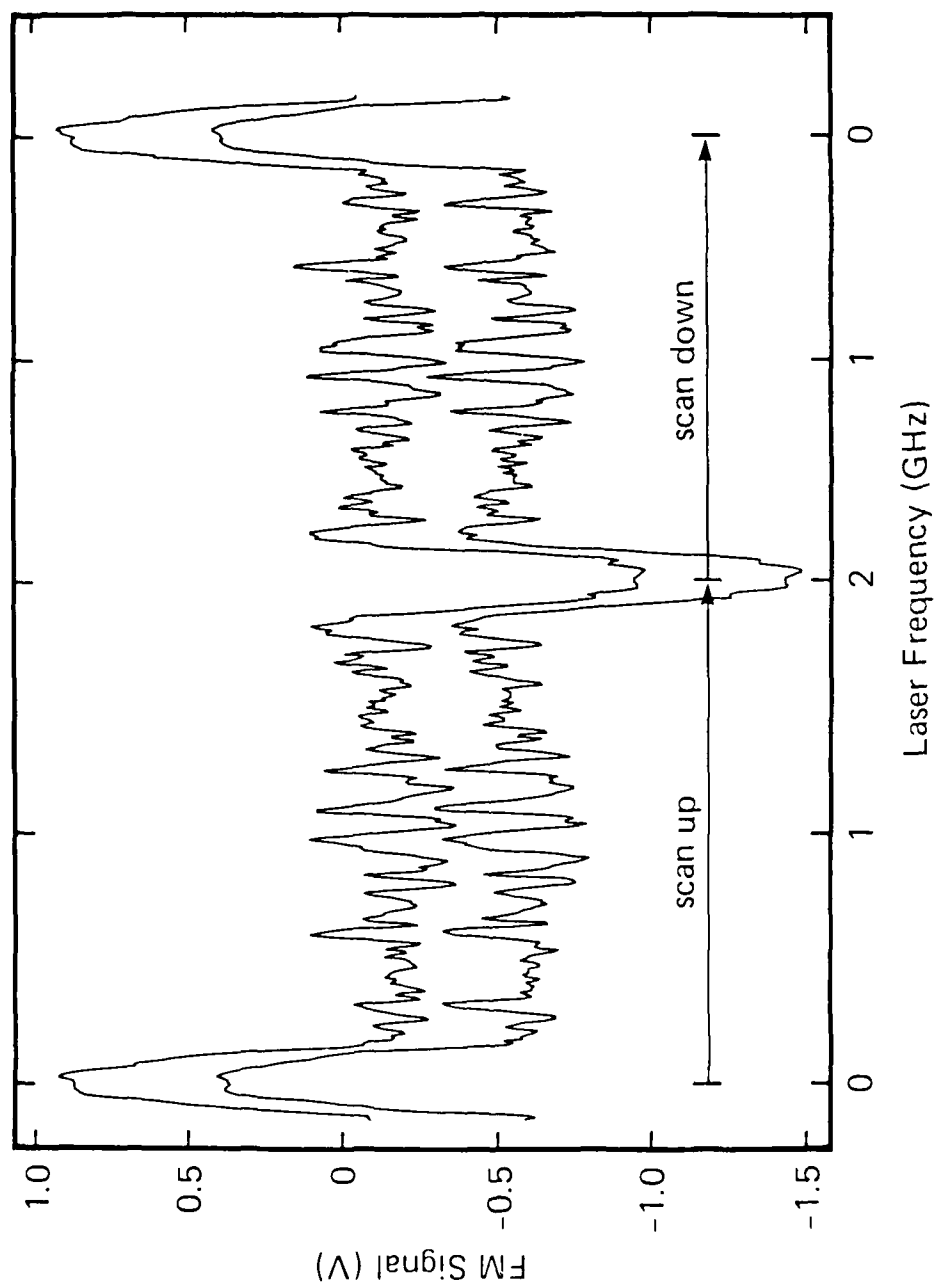
Figure 6
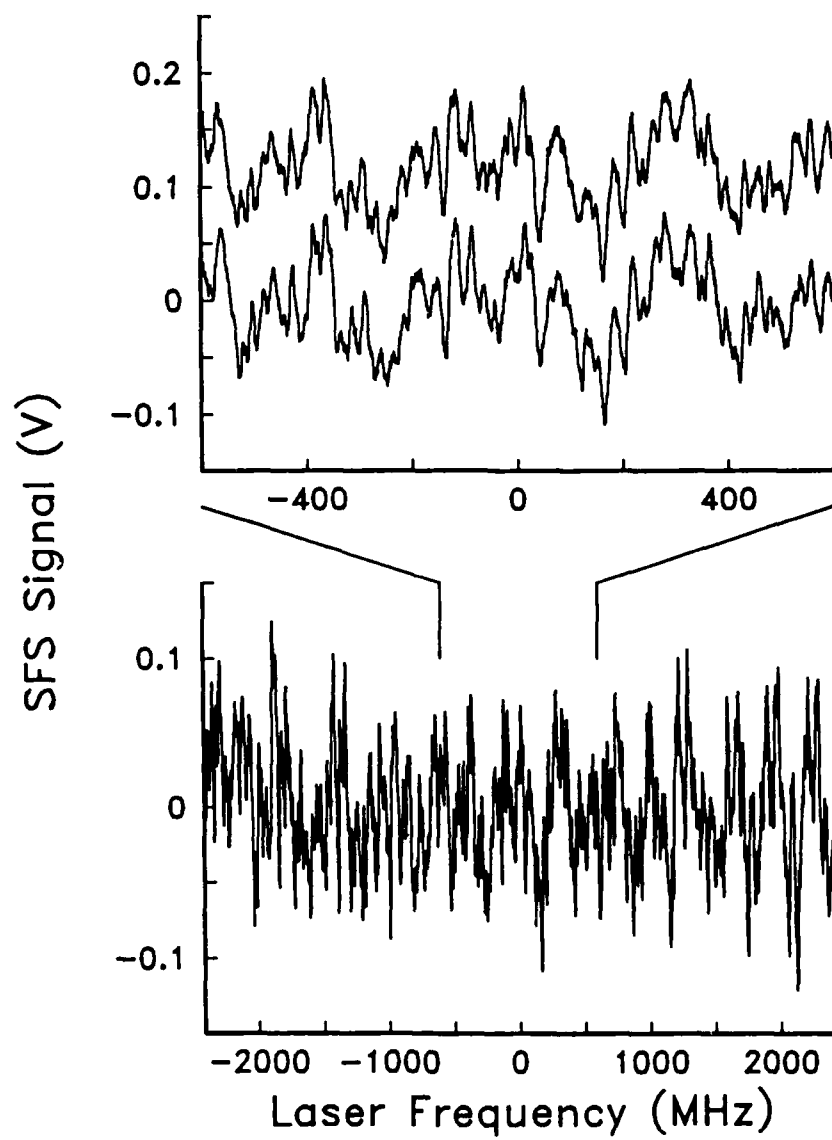
Figure 7
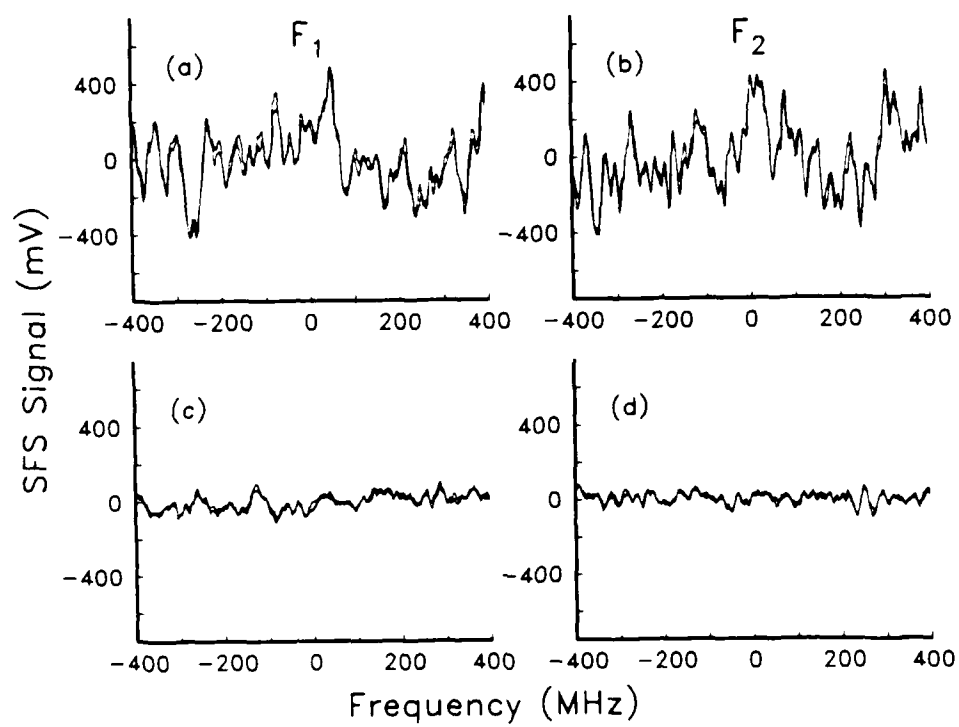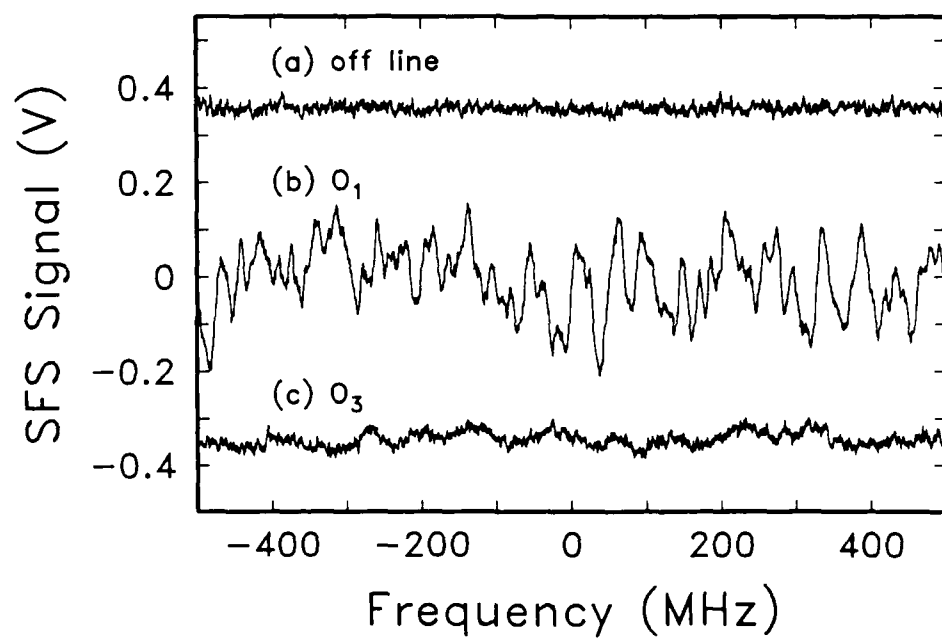
Figure 8
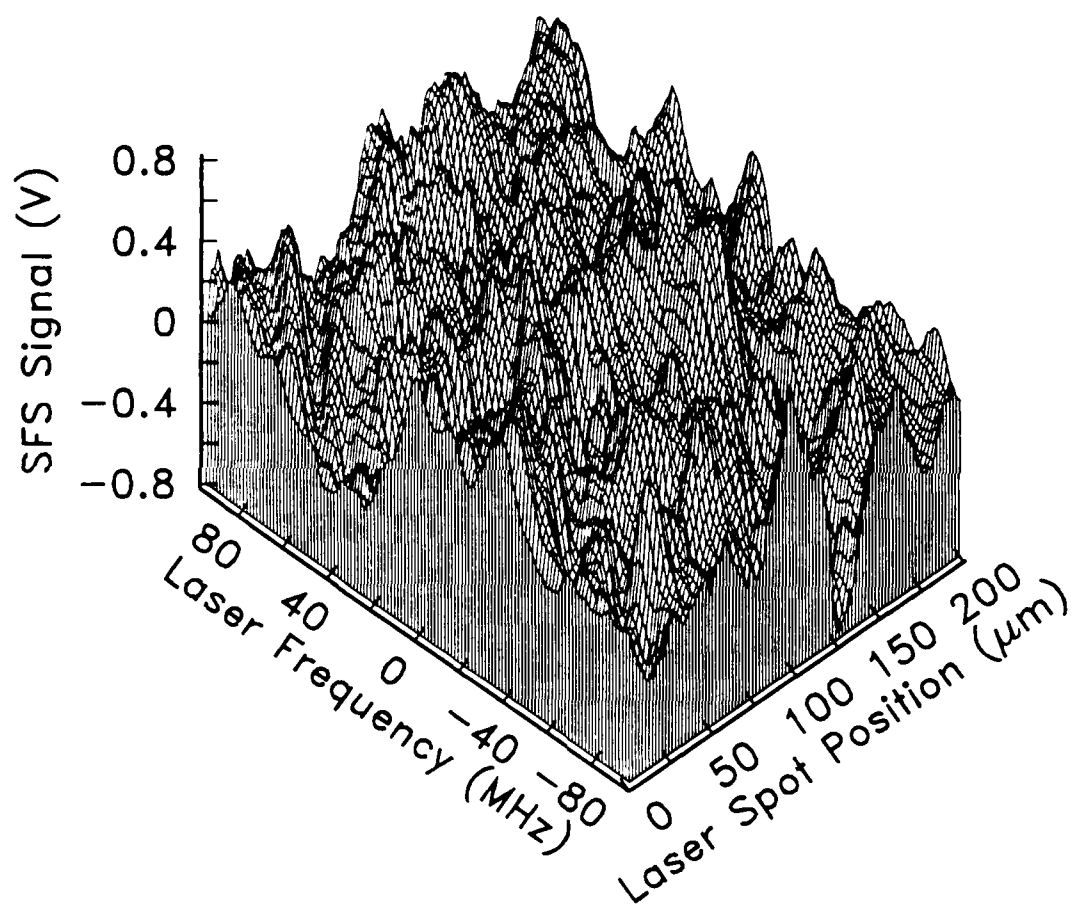
Figure 9

Figure 10

Figure 11

Figure 12
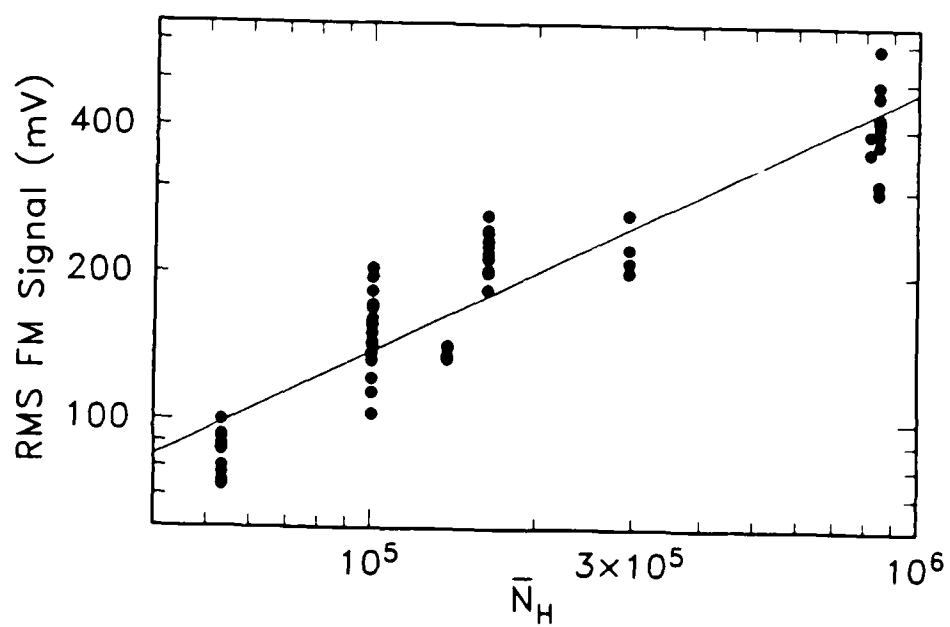
Figure 13
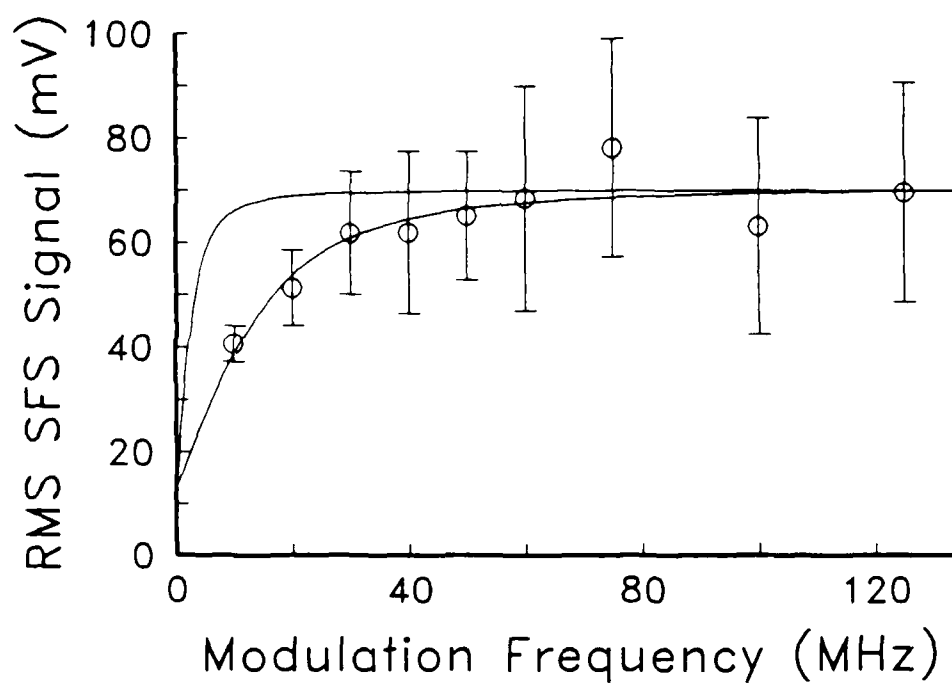
Figure 14
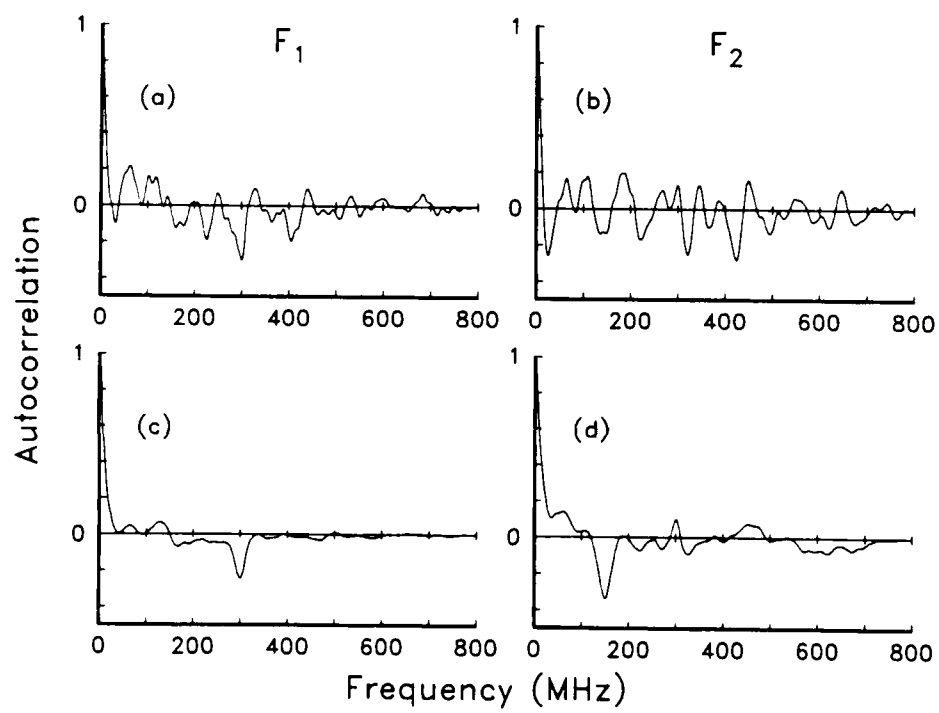
Figure 15

TECHNICAL REPORT DISTRIBUTION LIST, GEN

	No. Copies		No. Copies
Office of Naval Research Attn: Code 1113 800 N. Quincy Street Arlington, Virginia 22217-5000	2	Dr. David Young Code 334 NORDA NSTL, Mississippi 39529	1
Dr. Bernard Douda Naval Weapons Support Center Code 50C Crane, Indiana 47522-5050	1	Naval Weapons Center Attn: Dr. Ron Atkins Chemistry Division China Lake, California 93555	1
Naval Civil Engineering Laboratory Attn: Dr. R. W. Drisko, Code L52 Port Hueneme, California 93401	1	Scientific Advisor Commandant of the Marine Corps Code RD-1 Washington, D.C. 20380	1
Defense Technical Information Center Building 5, Cameron Station Alexandria, Virginia 22314	12 high quality	U.S. Army Research Office Attn: CRD-AA-IP P.O. Box 12211 Research Triangle Park, NC 27709	1
DTNSRDC Attn: Dr. H. Singerman Applied Chemistry Division Annapolis, Maryland 21401	1	Mr. John Boyle Materials Branch Naval Ship Engineering Center Philadelphia, Pennsylvania 19112	1
Dr. William Tolles Superintendent Chemistry Division, Code 6100 Naval Research Laboratory Washington, D.C. 20375-5000	1	Naval Ocean Systems Center Attn: Dr. S. Yamamoto Marine Sciences Division San Diego, California 91232	1

END

DATE

FILMED

5-88

DTIC